

Relating the Diffusion of Small Ligands in Human Neuroglobin to Its Structural and Mechanical Properties

Anthony Bocahut,[†] Sophie Bernad,[‡] Pierre Seban,[‡] and Sophie Sacquin-Mora^{*,†}

Laboratoire de Biochimie Théorique, UPR 9080 CNRS Institut de Biologie Physico-Chimique, 13 rue Pierre et Marie Curie, 75005 Paris, France, Laboratoire de Chimie Physique, Université Paris-sud 11, CNRS UMR8000 Bât. 350, 91405 Orsay, France

Received: July 20, 2009; Revised Manuscript Received: October 24, 2009

Neuroglobin (Ngb), a recently discovered member of the globin family, is overexpressed in the brain tissues over oxygen deprivation. Unlike more classical globins, such as myoglobin and hemoglobin, it is characterized by a hexacoordinated heme, and its physiological role is still unknown, despite the numerous investigations made on the protein in recent years. Another important specific feature of human Ngb is the presence of two cysteine residues (Cys46 and Cys55), which are known to form an intramolecular disulfide bridge. Since previous work on human Ngb reported that its ligand binding properties could be controlled by the coordination state of the Fe²⁺ atom (in the heme moiety) and the redox state of the thiol groups, we choose to develop a simulation approach combining coarse-grain Brownian dynamics and all-atom molecular dynamics and metadynamics. We have studied the diffusion of small ligands (CO, NO, and O₂) in the globin internal cavity network for various states of human Ngb. Our results show how the structural and mechanical properties of the protein can be related to the ligand migration pathway, which can be extensively modified when changing the thiol's redox state and the iron's coordination state. We suggest that ligand binding is favored in the pentacoordinated species bearing an internal disulfide bridge.

Introduction

The globin family is present in the three domains of life, and its classical representatives, hemoglobin (Hb) and myoglobin (Mb), have been widely investigated for more than four decades. These small respiratory proteins are characterized by a highly conserved α -helical fold and the ability to reversibly bind dioxygen and other small ligands at the central iron of a proto-heme IX prosthetic group.^{1–5} A newcomer in this large family, the recently discovered neuroglobin (Ngb) is predominantly expressed in the brain and nerve tissues of vertebrates⁶ under hypoxia or ischemia. Even though this single chain of 151 amino acids has less than 25% sequence identity with its more prominent cousins Hb and Mb, Ngb nevertheless displays all the key determinants of the globin fold.^{7–9} In the absence of an external ligand, the main structural characteristic of Ngb is the hexacoordination of the heme iron, which is bound by the proximal histidine in the F helix His96-F8 and the distal histidine in the E helix His64-E7, whereas Hb and Mb are both pentacoordinated globins with only the proximal histidine bound to the iron. In the case of the hexacoordinated Ngb, an external ligand would have to compete with His64 for the coordination of Fe²⁺. This feature has been proposed as a novel mechanism for the regulation of ligand affinity in heme proteins,^{10,11} but its functional significance is still not understood.

More generally, the physiological function of Ngb has remained elusive over the years.^{12–15} Because of its low expression level and moderate affinity for O₂ in neuronal cells, a simple storage or carrier function is usually considered unlikely. Numerous experimental studies have led to the

development of several hypotheses regarding the role of Ngb in the brain,^{16–20} particularly as a neuroprotectant, since its overexpression under low pressure of oxygen increases the recovery from stroke in experimental animals.^{21–23} Alternative functions for Ngb, such as signaling of hypoxia, radical scavenging, or detoxification of O₂ or NO derived species, were also proposed, but still not as definitive physiological roles.¹⁵

Neuroglobin presents two other remarkable structural attributes as compared to the more familiar Hb and Mb. First, in carboxy murine neuroglobin, ligand binding is associated with a large sliding movement of the heme toward the interior of the protein and an extensive reorganization of its internal cavities^{24–26} (instead of a more classical swinging motion of the distal histidine). Another interesting feature of human Ngb (which is absent from the murine Ngb) is the presence of two cysteine residues located in the CD loop, Cys46-CD7 and Cys55-D5, which are susceptible to forming an intramolecular disulfide bridge under oxidizing conditions. Experimental²⁷ and computational^{28,29} works have shown how the elimination of this bridge lowers the distal histidine dissociation rate, yielding a similar decrease in the O₂ affinity. All these observations led to a complex picture of the structural and ligand binding properties of Ngb.

The small cavity network located in the matrix of globular proteins usually plays a key role in ligand migration and for the control of protein function.^{30,31} In the case of globins, the diffusion pathways of various ligands have been extensively studied over the last years,^{32–42} showing great variability among the different members of this protein family.⁴³ In this work, we used a computer simulation approach to investigate how the aforementioned characteristics of human Ngb can influence the diffusion of small gaseous ligands in the protein; in particular, by changing the structural and mechanical properties of the internal cavity network. We first performed all-atom molecular

* Corresponding author. Phone: +33-1-58-41-51-65. Fax: +33-1-58-41-50-26. E-mail: sacquin@ibpc.fr.

[†] Institut de Biologie Physico-Chimique.

[‡] Université Paris-sud.

dynamics (MD) and coarse-grain Brownian dynamics (BD) simulations for various coordination (penta or hexa) and thiol group redox (with or without disulfide bridge) states of wild type human Ngb to obtain a complete picture of the conformational states that are accessible to the protein. In a second step, we explored the diffusion of small ligands, such as CO, NO, and O₂, in human Ngb via metadynamics simulations performed on the different conformations of Ngb that had been produced at the earlier stage of the study. The resulting free-energy surfaces (FESs) show how the iron coordination and the thiols redox state in the protein substantially affect the ligand diffusion path in human Ngb and how ligand binding is clearly favored in the pentacoordinated structure of Ngb bearing a disulfide bridge.

Materials and Methods

The starting coordinates employed for the simulations were taken from the experimental X-ray structure of human Ngb at 1.95 Å resolution (PDB entry 1OJ6,⁸ B-chain). To begin with, we performed three mutations in silico (G46C, S55C, and S120C) to retrieve the wild type cysteines that are not present in the crystal. All simulations were performed in the Fe²⁺, reduced state of the iron metal atom of the heme group.

Classical Molecular Dynamics. MD simulations were performed with the Gromacs^{44–46} software package using the OPLS all atoms force field.⁴⁷ Quantum chemical calculations with Gaussian⁴⁸ were performed to determine the charges of the hexacoordinated heme group using the B3LYP⁴⁹ and the 6-31G* basis sets. The other force field parameters for the prosthetic group were taken from previous studies done on Mb.⁵⁰ The protein was solvated in a cubic box of side length 78 Å, using periodic boundary conditions, with explicit single-point charge water molecules.⁵¹ Six Na⁺ ions were added to neutralize the system, which contained a total of around 48 000 atoms. All simulations were performed at 1 atm and 300 K, maintained with the Berendsen barostat and thermostat.⁵² Long-range electrostatic interactions were treated using the particle mesh Ewald method,⁵³ with a grid spacing of 0.12 nm and a nonbonded pair list cutoff of 9.0 Å with an updating of the pair list every five steps. We chose a time step of 2 fs by constraining bond lengths involving H atoms with the LINCS algorithm.⁵⁴ The solvent was first relaxed by an energy minimization, which was followed by a 100 ps equilibration step under restraint, and then heated slowly to 300 K. Production runs (25 ns) were then performed, from which the last 20 ns were kept for analysis. In particular, the MD trajectories were investigated using principal component analysis (PCA)^{55–58} on the eight first normal modes of the protein to retrieve the most significant residue fluctuations occurring along the collective modes of motion of the Ngb.

The online software Pocket Finder (<http://www.modeling.leeds.ac.uk/pocketfinder/>)⁵⁹ was used for detecting cavities in the different structures of Ngb that were produced and calculating their volumes. These calculations were performed on the clusterized structures resulting from the Gromacs post-treatment program with the heme prosthetic group, but in the absence of ligand.

Brownian Dynamics Simulations. BD simulations have been carried out using the ProPHet (Probing Protein Heterogeneity) program.^{60,61} The simulations used a coarse-grained protein model, in which each amino acid is represented by one pseudoatom located at the C_α position and either one or two (for larger residues) pseudoatoms replacing the side chain (with the exception of Gly).⁶² Interactions between the pseudoatoms are treated according to the standard elastic network model;⁶³

that is, all pseudoatoms lying closer than 9 Å are joined with quadratic springs having the same force constant of 0.6 kcal mol⁻¹ Å⁻². Springs are assumed to be relaxed in the reference conformation of the protein, derived either from the crystallographic data or from the clusterized structures produced by the MD simulations. The heme group was also represented in the reduced model via one pseudoatom located in the center of each of the four rings of the porphyrin and one pseudoatom for the central iron atom. The simulations use an implicit solvent representation via the diffusion and random displacement terms in the equation of motion,⁶⁴ and hydrodynamic interactions are included through the diffusion tensor.⁶⁵

From the positional fluctuations resulting from BD simulations, carried out for 50 000 steps at a temperature of 300 K, effective force constants for displacing each particle *i* are calculated as

$$k_i = \frac{3k_B T}{\langle (d_i - \langle d_i \rangle)^2 \rangle} \quad (1)$$

where brackets $\langle \rangle$ indicate an average taken over the whole simulation; k_B is the Boltzmann constant; and d_i is the average distance of particle *i* from the other particles *j* in the protein, excluding the pseudoatoms, which belong to the same residue *m* to which particle *i* belongs. In addition, the distances between the C_α pseudoatom of residue *m* and the C_α pseudoatoms of the adjacent residues *m* + 1 and *m* − 1 are not included in the average. The force constant associated with each residue *m* is taken to be the average of the force constants calculated according to eq 1 for each of the pseudoatoms *i* forming this residue. Within this framework, the mechanical properties of the protein are described at the residue level by its “rigidity profile”; that is, by the ordered sequence of the force constants calculated for each residue.

Metadynamics. The metadynamics⁶⁶ method (see ref 67 for a recent and extensive review) is a biased dynamic that is able to simulate rare events and reconstruct FESs along a set of collective variables (CVs) using a history-dependent potential. Here, we used the Plumed⁶⁸ package (<http://merlino.mi.infn.it/~plumed/PLUMED/Home.html>), a portable plug-in which can be included in the Gromacs software. During the simulation, an external potential is added, which disfavors configurations in the collective variables space, $S(r)$, that have already been visited, and is constructed as a sum of Gaussians centered around the values of the $s(t)$ explored during the dynamics,

$$V_G(S(r), t) = w \sum_{t' = \tau_G, 2\tau_G, \dots, t' < t} \exp\left(-\frac{(S(r) - s(t'))^2}{2\delta s^2}\right) \quad (2)$$

where $s(t) = S(r(t))$ is the value of the CVs at time *t*. To describe this potential, V_G , three parameters are used: the Gaussian height, w ; the Gaussian width, δs ; and the deposit frequency of the Gaussian τ_G . Eventually, the free energy of the system is given by

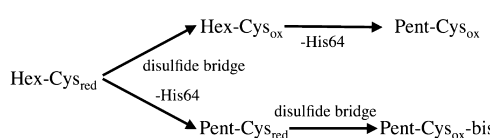
$$\lim_{t \rightarrow \infty} V_G(s, t) \approx -F(s) \quad (3)$$

To form the Cys-oxidized (Cys_{ox}) species of Ngb (where Cys46-CD7 and Cys55-D5 are bound by a disulfide bridge), we performed metadynamics calculations using the S–S distance of the cysteine chains as the only collective variable until the residues were sufficiently close and then equilibrated the resulting structure via MD simulations while including a

covalent S–S bond in the force field. We also used metadynamics simulations to investigate the migration of small gaseous ligands in the internal cavities network of human Ngb. The ligand charges were obtained from density functional calculations: For CO, $0.17e$ for the carbon and $-0.17e$ for the oxygen; for NO, $0.11e$ on the nitrogen and $-0.11e$ on the oxygen; for O_2 , $0.0e$ on both atoms. For each metadynamics simulation, the initial positioning of the ligand in the protein was performed using interactive simulations via the MDDRiver⁶⁹ software library. The heme Fe-ligand distance and the His96(NE2 atom)–heme(Fe atom)–ligand angle were chosen as the CVs for all the calculations, with a Gaussian height, w , of 0.2 kJ mol^{-1} and a deposit time of 400 fs , and the Gaussian width was determined by the well-tempered⁷⁰ directive to guarantee the convergence of the simulations. To extensively explore the cavity network, we also used the multiple walkers⁷¹ directive, which permits running simulations on multiple replicas of the system simultaneously, with several initial positions for the ligand in the protein.

Results

Production and Structural Comparison of Five Different Ngb States. Starting from Ngb in its hexacoordinated, reduced (without disulfide bridge) state (Hex-Cys_{red}), we could either form a pentacoordinated reduced state (Pent-Cys_{red}) by removing the constraint on the distance between the heme and the distal histidine (His64-E7) during MD simulations or form a disulfide bridge between Cys46-CD7 and Cys55-D5 via metadynamics simulations to obtain a hexacoordinated oxidized state (Hex-Cys_{ox}). A pentacoordinated oxidized state can then be formed either by severing the Fe-distal histidine bond in the Hex-Cys_{ox} state, leading to the Pent-Cys_{ox} state, or by building a disulfide bridge in the Pent-Cys_{red} state, again using metadynamics, leading to a state named Pent-Cys_{ox}-bis. The production of these various states of human Ngb can be summarized as follows:



Note that with this production scheme, our Pent-Cys_{ox} state corresponds to the 5c-Cox state studied in the work of Nadra et al.²⁸ For the production of the oxidized states, the free-energy profiles obtained from the metadynamics simulations on Hex-Cys_{red} and Pent-Cys_{red} gave us two metastable states with S–S distances of 7 and 4 \AA , respectively, which were used as the starting point for the MD simulations of the Hex-Cys_{ox} and Pent-Cys_{ox}-bis states, thus suggesting that the disulfide bridge might be easier to form in the pentacoordinated state of the protein.

The root-mean-square deviation of the $C\alpha$ atoms in the simulation of the Hex-Cys_{red} state reaches values of around 1.4 \AA with respect to the original crystallographic structure. The structural alignment of the various states is represented in Figure 1. Whereas the overall globin fold is well-conserved throughout all five Ngb 3D structures, we can see how the final position of the heme prosthetic group in the pentacoordinated-oxidized states (Pent-Cys_{ox} and Pent-Cys_{ox}-bis) strongly depends on the mechanism of formation of this state. This is emphasized by the data presented in Table 1, which shows the Fe and heme-CHC atom displacements in our five structures as compared to the crystal structures of the hexacoordinated⁹ and CO-bound²⁴ murine Ngb. In the first formation pathway (leading to Pent-

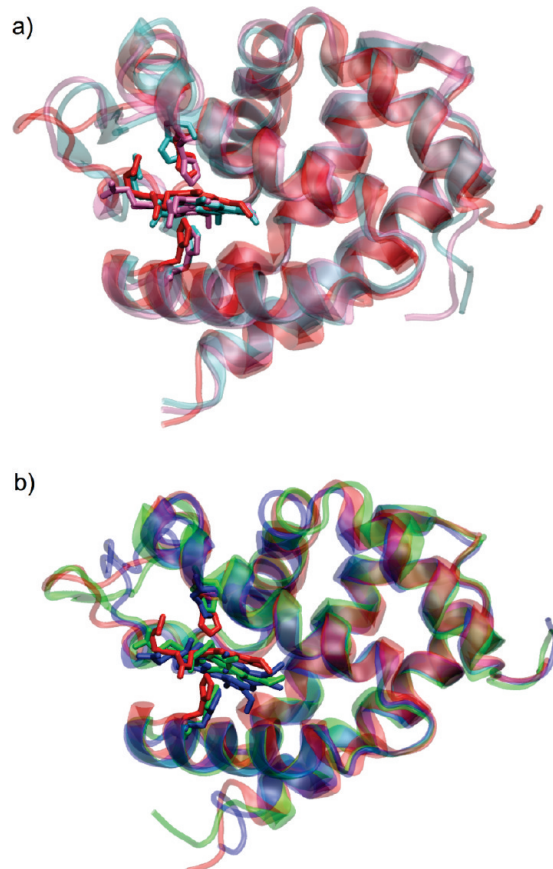


Figure 1. A cartoon representation of the different states of Ngb, the heme group and the binding histidines. (a) Structural alignment of the Hex-Cys_{red} (red), Hex-Cys_{ox} (pink) and Pent-Cys_{ox} (cyan) states. (b) Structural alignment of the Hex-Cys_{red} (red), Pent-Cys_{red} (green) and Pent-Cys_{ox}-bis (blue) states. The images in this figure and Figures 2, 5 and 6 were prepared using Visual Molecular Dynamics.⁷⁷

TABLE 1: Displacements of the Fe and CHC Atoms (in \AA) for the Five Ngb States with Respect to the Crystal Structures of Hexacoordinated and C-Bound Murine Ngb

structure	hexa murine Ngb		CO-bound murine Ngb	
	dFE	dCHC	dFE	dCHC
Hex-Cys _{red}	0.67	0.79	2.80	3.12
Hex-Cys _{ox}	0.68	0.54	2.26	3.03
Pent-Cys _{ox}	0.40	0.55	1.93	2.39
Pent-Cys _{red}	1.11	1.35	1.29	1.68
Pent-Cys _{ox} -bis	2.05	3.02	0.33	1.06

Cys_{ox} via Hex-Cys_{ox}), the heme movement is extremely limited, with displacements inferior to 0.7 \AA for the Hex-Cys_{ox} and Pent-Cys_{ox} states and a position of the heme group that is much closer to the Hex than to the CO-bound murine Ngb structure in both cases. The results are in close agreement with the data obtained by Nadra et al.²⁸ In contrast, the second formation pathway (leading to Pent-Cys_{ox}-bis via Pent-Cys_{red}) induces an important heme sliding movement initiated by the severing of the His-Fe bond and the formation of the Pent-Cys_{red} state and further continued upon building of the disulfide bridge. This alternative mechanism eventually gives displacements for the Fe and CHC atom of 2.05 and 3.02 \AA , respectively, in the Pent-Cys_{ox}-bis state, which are comparable to the 2.0 and 3.04 \AA displacements that were obtained experimentally.²⁴

Exploring the Internal Cavities Network. The different species of Ngb show the presence of several internal cavities that could be related to the xenon cavities (Xe1, Xe2, Xe3, and

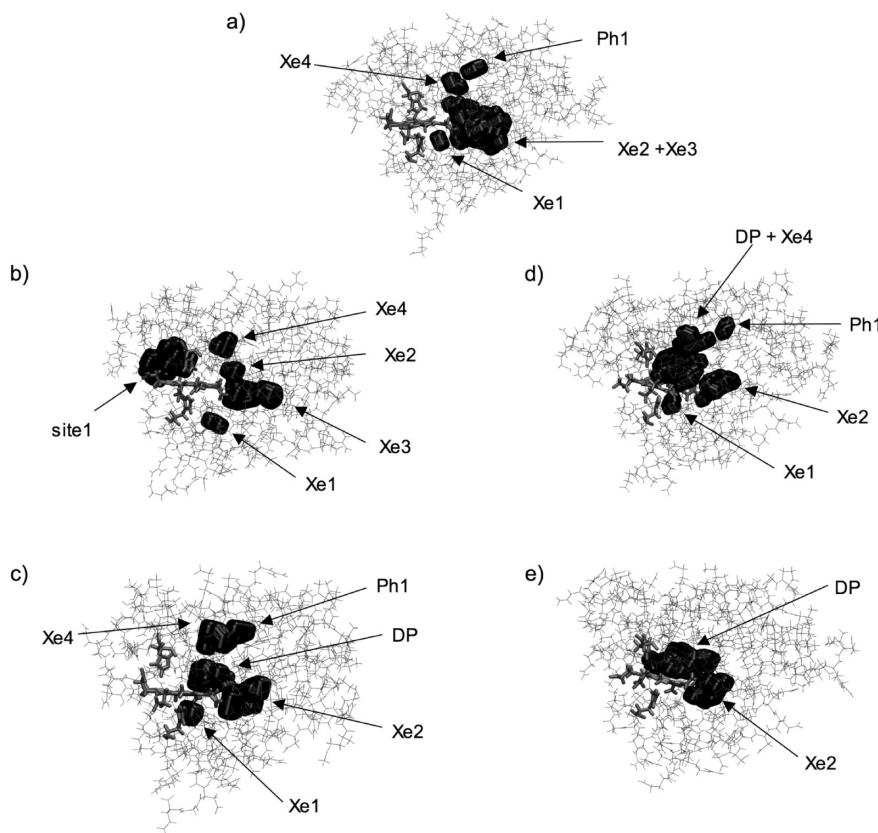


Figure 2. Main cavities in the different structures of human Ngb detected by the online software Pocket Finder.⁵⁹ (a) Hex-Cys_{red}, (b) Hex-Cys_{ox}, (c) Pent-Cys_{ox}, (d) Pent-Cys_{red}, (e) Pent-Cys_{ox}-bis.

TABLE 2: Volume (in Å³) of the Main Internal Cavities Found with the Pocket Finder Software for the Five Ngb States

	Xe1	Xe2	Xe3	Xe4	DP	Ph1	total
Hex-Cys _{red}	10	330	24		20	385	
Hex-Cys _{ox}	16	96	35	23			170
Pent-Cys _{ox}	21	110		12	76	53	271
Pent-Cys _{red}	15	102		262	25		419
Pent-Cys _{ox} -bis		79		160			239

Xe4) and the distal pocket (DP) that have been observed experimentally in sperm whale Mb³⁰ and to the phantom1 cavity (Ph1) that was detected in the same protein by MD simulations.^{35,36} However, we can see from Figure 2 and Table 2, which summarizes the cavities volumes in each state, that changes in the iron coordination and cysteines redox states induce considerable reorganization of the cavity network. The Hex-Cys_{red} (see Figure 2a) state shows a predominant Xe2/Xe3 cavity with a volume of 330 Å³ (over a total of 385 Å³), similar to what is observed in murine metNgb, in both simulations²⁵ and recent experiments with Xe.⁷² The formation of the disulfide bridge to form the Hex-Cys_{ox} state then leads to an important reduction in the volume of the Xe cavities (which now occupy only 170 Å³) and to the creation of a new large pocket of 167 Å³ (termed site 1 in Figure 2b) surrounded by the CD loop. Notably, although site 1 does not correspond to any of the known Xe cavities of Mb, its equivalent has very recently been observed in a Xe adduct of human Hb.⁷³ After severing the His–Fe bond to form the Pent-Cys_{ox} state (Figure 2c), the site1 pocket disappears, and the Xe sites partially regain their initial volume to reach a total of 271 Å³. If we follow the second mechanism and first form the Pent-Cys_{red} state of Ngb, we can observe a large increase in the total cavity volume (419 Å³) and a

restructuring of the tunnel network toward the upper part of the protein, where the DP/Xe4 site is now prevailing with a volume of 262 Å³ (see Figure 2d). Finally, the Pent-Cys_{ox}-bis state presents a reduced network (occupying only 239 Å³), which consists essentially of the Xe2 and DP cavities and is comparable to the one obtained for murine Ngb.²⁵ One can note that in both mechanisms, the transition to a pentacoordinated state induces an important increase in the Xe, DP, and Ph1 total cavity volume, like that previously observed both experimentally and theoretically for murine Ngb,^{24,25} whereas the formation of the disulfide bridge is always associated with a decrease of the same volume.

Mechanical Properties of Neuroglobin. The force constant profile obtained from the crystallographic structure of human neuroglobin⁸ (PDB code 1OJ6) is plotted in Figure 3a. Similar to what has been observed in our previous study on hemoproteins,⁶⁰ the series of rigidity peaks reflects the α-helical fold of the protein with two flexible regions corresponding to the CD (41–51) and EF (77–85) loops. Furthermore, the rigidity peaks are strongly correlated with the conserved positions in the protein sequence. In their work of 1999 made on 728 sequences of different globin subfamilies (which did not include neuroglobin), Ptitsyn and Ting⁷⁴ identified 13 conserved heme-binding residues. It turns out that 12 out of these 13 residues (which are indicated by empty squares on Figure 3a) actually belong to rigid regions of the protein. This suggests how important the tight binding of the prosthetic group is for the biological activity of the protein.⁶¹ Likewise, the five residues forming the folding nucleus of Ngb (black circles in Figure 3a) correspond to rigidity peaks, thus underlying the strong correspondence between a protein's mechanics and its functional and structural properties. Another interesting feature of the rigidity profile is the presence of peaks corresponding to Tyr88, Leu89, and Leu92 (which

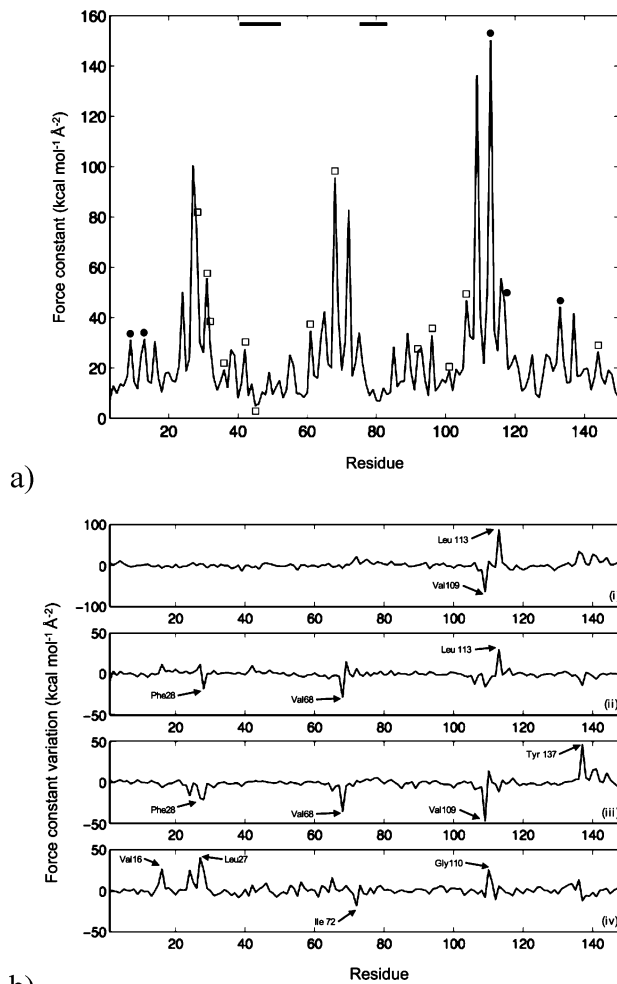


Figure 3. (a) Rigidity profile (in $\text{kcal mol}^{-1} \text{\AA}^{-2}$) of human Ngb in the Hex-Cys_{red} state. Squares indicate heme-binding conserved residues of globins (from left to right: Phe28-B10, Leu31-B13, Phe32-B14, Pro36-C2, Phe42-CD1, Asn45-CD4, Phe61-E4, Val68-E11, Leu92-F4, His96-F8, Val101-FG5, Phe106-G5, Met144-H19), and black circles indicate the conserved folding nucleus (from left to right: Ile9-A8, Trp13-A12, Leu113-G12, Leu117-G16, Trp133-H8). The two black horizontal bars at the top of the figure indicate the position of the CD and EF loops along the sequence. (b) Modifications in the force constant profile upon changing the Ngb state: curve i, from the Hex-Cys_{red} to the Hex-Cys_{ox} state; curve ii, from the Hex-Cys_{ox} to the Pent-Cys_{ox} state; curve iii, from the Hex-Cys_{red} to the Pent-Cys_{red} state; curve iv, from the Pent-Cys_{red} to the Pent-Cys_{ox}-bis state.

belongs to the group of conserved heme-binding residues), since recent NMR experiments have shown how hydrophobic interaction between these three residues, which are specific to neuroglobin, could contribute to stabilize the secondary structure of helix F.⁷⁵

The flexibility profile of Ngb has been obtained by computing the root-mean-square fluctuation (RMSF) along the protein sequence via a PCA approach using the first eight normal modes of the proteins (which characterize over 99% of the protein fluctuations). As we can see in Figure 4a, the most flexible parts of the protein are located in the CD and EF loops, in agreement with the simulations made on human Ngb by Nadra et al.²⁸

The modifications in the rigidity and flexibility profiles of Ngb upon changing the iron coordination state or the redox state of the thiol groups are plotted in Figures 3b and 4b, respectively. Remarkably, the most important changes in these profiles concern residues defining the frontiers between internal cavities

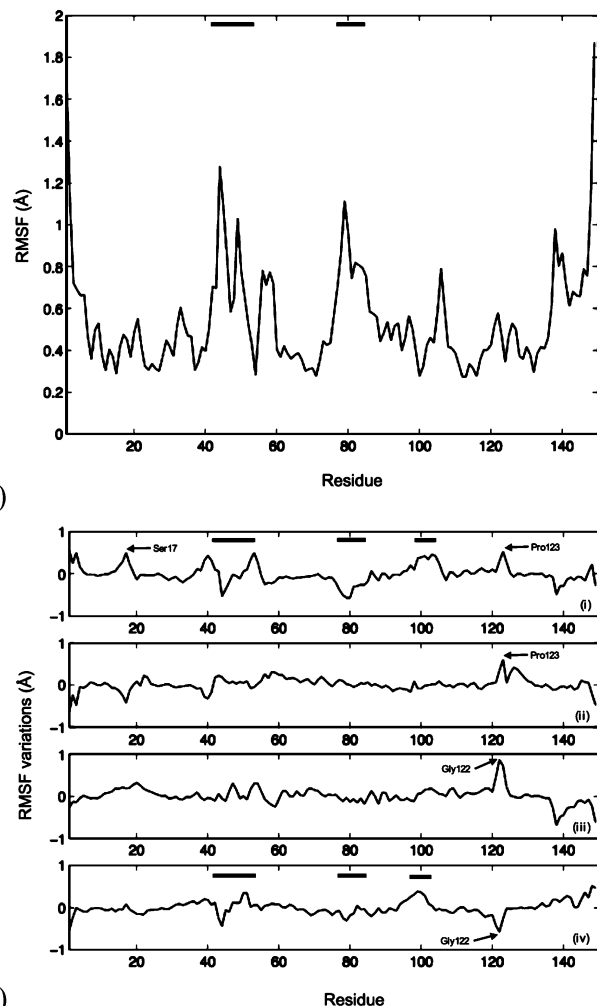


Figure 4. (a) RMSF (in Å) along the sequence obtained via PCA on the first eight normal modes of human neuroglobin in the Hex-Cys_{red} state. The two black horizontal bars at the top of the figure indicate the position of the CD and EF loops along the sequence. (b) Modifications of the flexibility profile upon changing the Ngb state: curve i, from the Hex-Cys_{red} to the Hex-Cys_{ox} state; curve ii, from the Hex-Cys_{ox} to the Pent-Cys_{ox} state; curve iii, from the Hex-Cys_{red} to the Pent-Cys_{red} state; curve iv, from the Pent-Cys_{red} to the Pent-Cys_{ox}-bis state. The black horizontal bars at the top of curves i and iv indicate the position of the CD, EF, and FG loops along the sequence.

or residues involved in the connection between these cavities and the external surface of the protein. For example, in curve iii in Figure 2b, which displays the change in rigidity when going from the Hex-Cys_{red} to the Pent-Cys_{red} state, the three residues showing the largest decrease in their force constant are Phe28-B10, Val68-E11, and Val109-G8, which are all located at the frontier between the DP and Xe4 cavities in Mb^{35,36} and Ngb.^{25,35,36,42} On the other hand, the residue undergoing the strongest rigidity increase is Tyr137-H12, which is involved in one of the putative entry channels connecting the external solvent with the internal cavity network.^{8,9} Other residues showing important changes in their force constant in Figure 3b are Leu113-G12 from the Xe2/Xe4 border; Val16-A15 and Gly110-G9, which have already been identified as taking part in ligand passageways in Hb;^{32,37} Leu27-B9, from the DP/Xe4 border; and Ile72-E5, from the Xe2/Xe3 border. Looking at the flexibility profiles of Figure 4b, we can notice that the formation of the disulfide bond in either the hexa or pentacoordinated states of the protein (curves i and iv) induces a clear decrease in the mobility of the CD and the EF loops

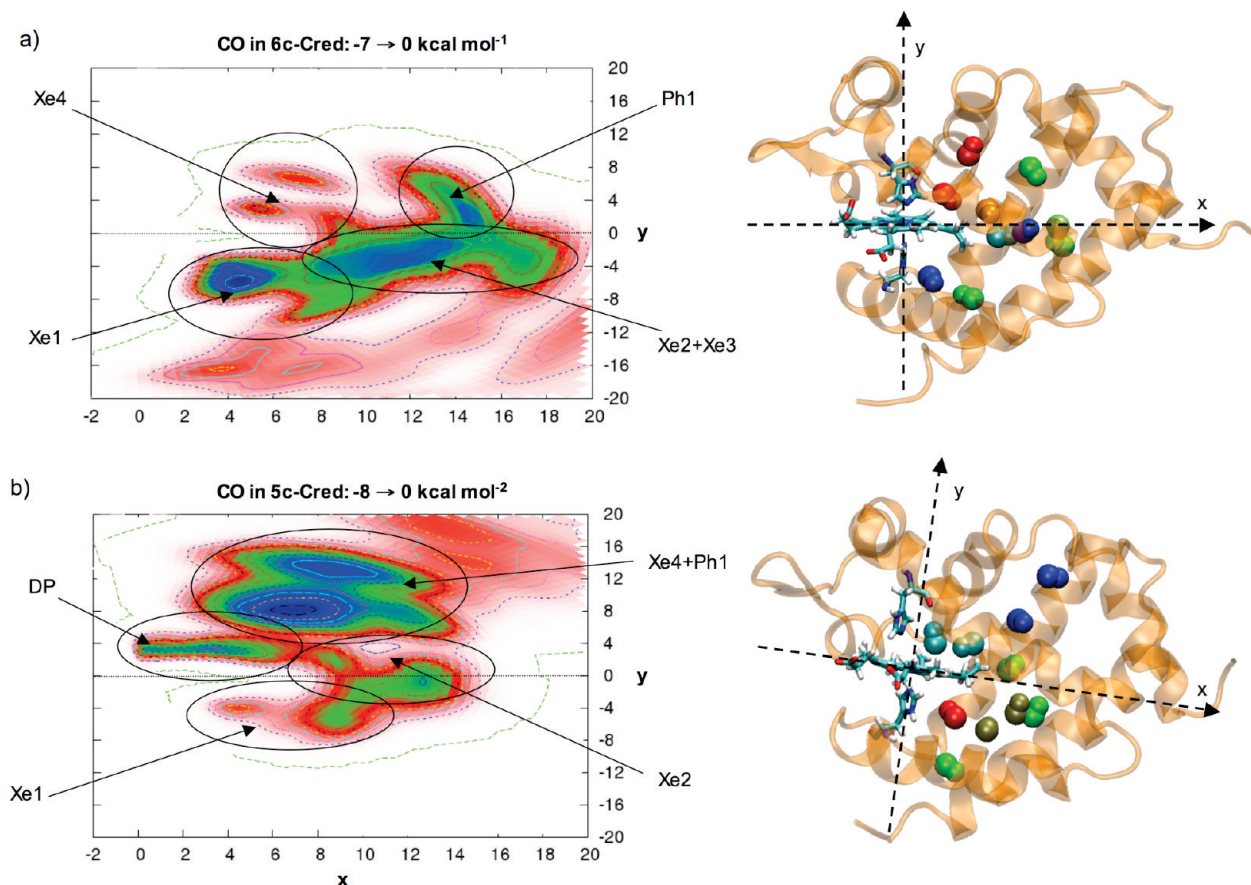


Figure 5. Left-hand side: free energy surfaces of the diffusion of CO in Ngb. We use a heme fixed coordinate with the iron atom as the origin, and the horizontal axis corresponds to the projection of the iron–ligand distance on the heme plane, whereas the vertical axis corresponds to the projection of the same distance on the axis orthogonal to the heme plane (see the axis representation in the figures on the right). The energy range is indicated for each surface, and blue and red areas correspond to the most negative and the least negative energies, respectively. This nomenclature is also used for Figures 7, 8, and 9. The black ellipses in this figure and Figure 7 highlight the position of the various cavities on the FES. Right hand side: a cartoon representation of Ngb with the most populated positions of CO in the cavities plotted as van der Waals spheres. The ligand color matches the energy levels indicated in the corresponding FES. (a) CO in the Hex-Cys_{red} state, (b) CO in the Pent-Cys_{red} state.

TABLE 3: Location of the Eight Ligand Exit Pathways Observed via Metadynamics Simulations of Small Ligands in Human Ngb

	residues	secondary structure elements
exit 1	Leu113, Leu114, Trp133, Ser134, Tyr 137	helices G and H
exit 2	Leu 92, Lys 95, His 96, and heme	heme and helix F
exit 3	Trp13, Val16, Ser19, Pro20, His23, Met 69, Met116	AB loop
exit 4	Leu103, Phe106, Val141, Met144, Ser145, Trp148	helices G and H
exit 5	Ala75, Leu82, Ser84, Leu85, Tyr88	EF loop
exit 6	Leu21, Glu22, His23, Gly24, Ile65, Arg66, Met69	helices B and E
exit 7	Arg3, Pro4, Val79, Glu80, Leu82, Leu136	N terminal and EF loop
exit 8	Phe28, Leu41, Phe42, Gln43, Tyr44, Phe61, His64, and heme	heme and CD loop

that seems to be compensated by a flexibility increase in the FG loop. Other interesting residues are Ser17-A16 and the Gly122-Pro123 pair from the GH loop, which circumscribe one of the ligand exit pathways in Hb.³⁷

Ligand Migration in the Cavity Network. We investigated the migration of CO, NO, and O₂ in each of the five Ngb states using metadynamics simulations with one to four starting positions of the ligand in the globin to extensively explore the accessible cavity network for each ligand and Ngb structure. The resulting free energy minima ranges (between -9 and 0 kcal mol⁻¹) obtained for the various cavity/ligand/Ngb state combinations agree well with previous simulations performed on Mb^{38–40} or Ngb.⁴²

CO Ligand. Starting with the Hex-Cys_{red} state, we can see in Figure 5a that the diffusion of CO is restricted to mainly the lower part of the globin (i.e., in cavities Xe1, Xe2 and Xe3),

TABLE 4: A Summary of the Ligand Exit Pathways Observed for CO, NO and O₂ in the Five States of Human Ngb

	Hex-Cys _{red}	Hex-Cys _{ox}	Pent-Cys _{ox}	Pent-Cys _{red}	Pent-Cys _{ox} -bis
CO	exits 1 and 2	exit 1	no exit	exit 3	exit4
NO	exit 4	exit 5	exit 4	exit 6	exits 1 and 6
O ₂	exit 6	exit 4	exit 7	exit 8	exits 4 and 6

thus reflecting the repartition of the cavity volumes previously observed in Figure 2a. The FES also allows to identification of two ligand exit pathways, termed exits 1 and 2 in Tables 3 and 4, which summarize all the ligand passageways toward the surface of the protein that were observed during the various metadynamics simulations. Although exit 1, which is located between helices G and H near Tyr137-H12 (see Figure 6b), has

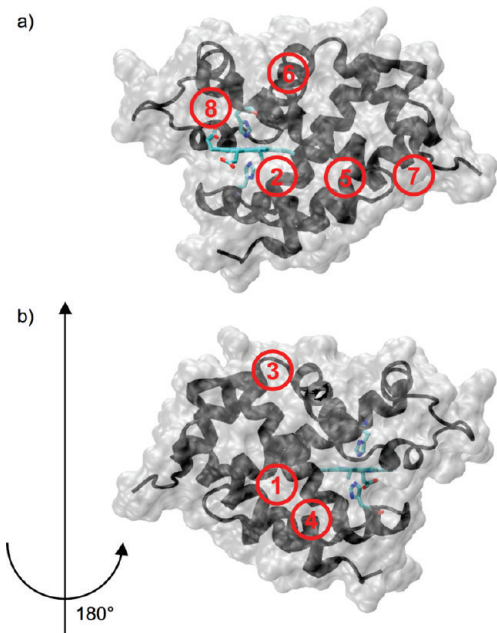


Figure 6. Cartoon (in black) and surface (in gray) representations of Ngb with the positions of the ligand exit pathways in red. (a) Front view, (b) back view. The precise locations of these exit pathways are detailed in Table 3.

already been identified as one entry channel connecting the inside of the protein with its surface,⁸ exit 2 is a newly identified pathway for Ngb situated on the proximal side between the heme and helix F (see Figure 6a), but a similar escaping trajectory has already been obtained for CO in Mb.⁴¹ In the Pent-Cys_{red} state (Figure 5b), the extensive reorganization of the cavity network induced by the heme sliding movement leads to a migration pathway of the ligand that now essentially visits the upper part of the protein (i.e., cavities Xe4, DP and Ph1), again agreeing with the distribution of cavities represented in Figure 2d. This reshaping of the protein internal structure leads to a new exit pathway for CO (termed exit 3), which is located around the AB loop (see Figure 6b) and can be related to ligand escape trajectories observed for simulations of Hb^{32,37} and Mb.⁴¹ The FESs of CO migration in the Pent-Cys_{ox}-bis, Hex-Cys_{ox}, and Pent-Cys_{ox} states are represented in Figure 7a, b, and c respectively. For the Pent-Cys_{ox}-bis state, the ligand chiefly occupies the most stable Xe2 and DP cavities, in agreement with the network plotted in Figure 2e and finally leaves the protein via the exit 4 pathway, which goes between helices G and H in the vicinity of Met 144 and can be related to the direct exit pathway from the Xe2 cavity observed by Cohen et al.³⁸ in Mb. In the Hex-Cys_{ox} state, the ligand again leaves the protein via the Xe3 cavity and exit1, but in the Pent-Cys_{ox} state, we did not observe any exit pathway because the simulations stopped while the ligand was attempting to leave the protein via the distal pathway^{38,40} and was blocked by His64-E7. Finally, we can also notice that the DP cavity (which prefigures ligand binding) is the most stable one in the Pent-Cys_{ox}-bis state (see Figure 7a).

NO Ligand. The FESs of NO migration in the five states of Ngb are plotted in Figure 8a–e. Once again, we can see how the hexa-to-penta-coordination transition for the heme induces a displacement of the ligand toward the upper cavities (DP and Xe4) of the protein and two new exit ligand passageways toward the protein's surface appear: In the Hex-Cys_{ox} state, NO leaves via exit 5, between Tyr88-F3 and the EF loop, and in the Pent-Cys_{red} and Pent-Cys_{ox}-bis states, the ligand uses exit 6 located

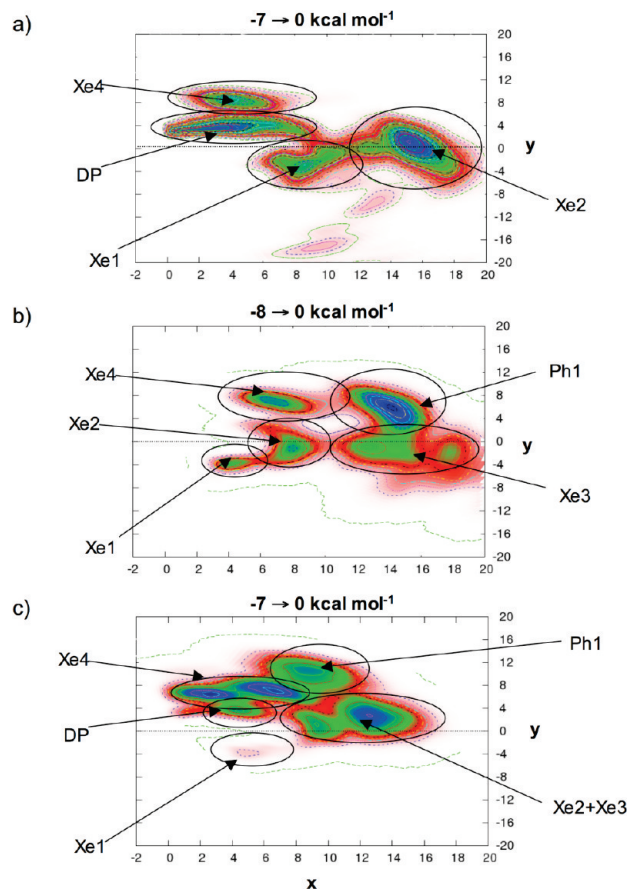


Figure 7. FESs of CO diffusion in Ngb. (a) Pent-Cys_{ox}-bis state, (b) Hex-Cys_{ox} state, (c) Pent-Cys_{ox} state.

at the top of the protein (see Figure 6). Interestingly, exit 5 was already identified in an earlier structural study of murine Ngb.⁹ Once more, the Pent-Cys_{ox}-bis state presents the most stable DP cavity (see Figure 8e). We can also notice a higher mobility of NO in the cavities as compared to CO, which can be explained by the smaller size of the ligand.

O₂ Ligand. The final group of FESs for the diffusion of O₂ in human Ngb is represented in Figures 9a–e. Remarkably, even though the ligand diffusion pathway changes significantly from one state to the other, Xe4 appears to be the most stable cavity in all cases. We could observe another two exits for O₂. In the Pent-Cys_{ox} state, the ligand leaves via exit 7, next to the N-terminal, which was also detected during simulations of CO in Mb.³⁹ More interestingly, in the Pent-Cys_{red} state, we can eventually see the ligand leave the protein past His64-E7 and through the CD loop via the classical distal pathway (termed exit 8 in Tables 3 and 4) that is commonly observed for Hb³⁷ and Mb.^{38,40,41} Another notable feature of O₂ migration is that it is the only ligand (probably because it is the smallest one and is not charged) for which we could obtain an almost ligand-bound configuration of Ngb when performing metadynamics simulations in the Pent-Cys_{ox} state (highlighted in Figure 9c), even though the DP cavity is more stable in the Pent-Cys_{ox}-bis state.

Discussion and Conclusions

In the present work, we have developed a theoretical approach that combines coarse-grain and all-atom dynamics simulations to investigate the relationship between the structural and mechanical properties of various states of human neuroglobin

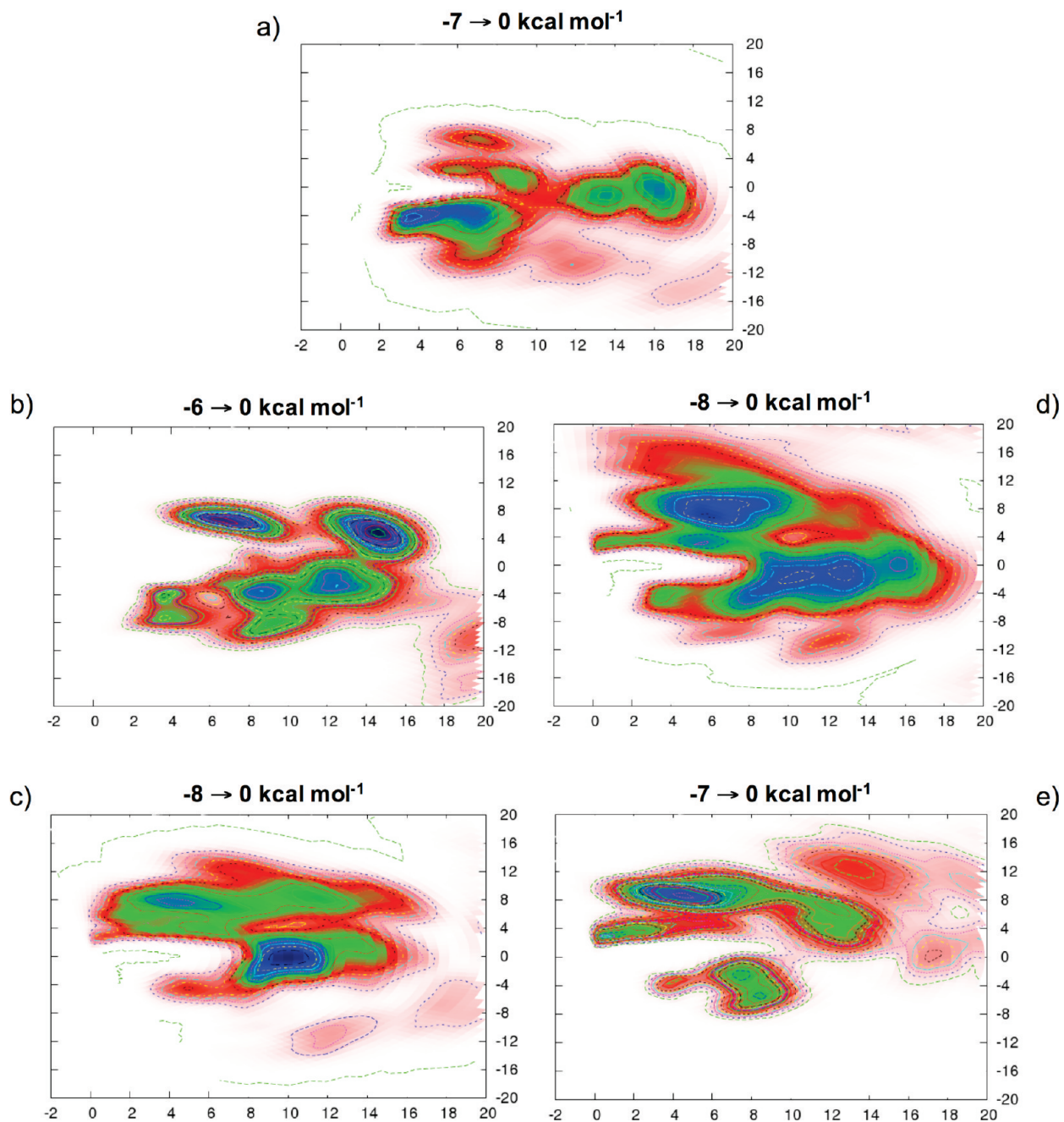


Figure 8. FESs of NO diffusion in Ngb, (a) Hex-Cys_{red} state, (b) Hex-Cys_{ox} state, (c) Pent-Cys_{ox} state, (d) Pent-Cys_{red} state, (e) Pent-Cys_{ox}-bis state.

and the diffusion of small ligands inside the protein internal cavity network. Starting from the crystallographic structure of human Ngb in its hexacoordinated state and with reduced cysteines in the CD loop, we used MD and metadynamics simulations to produce four other species presenting either a hexa or pentacoordinated heme iron and with or without an internal disulfide bridge between the two cysteines of the CD-loop. Looking at the structure of our five Ngb species, we could observe how the heme position inside the globin clearly depends on the mechanism that has been followed to form the considered state. In their work on human Ngb, Nadra et al.²⁸ observed only a limited sliding movement of the heme group upon formation of the pentacoordinated with the oxidized thiol groups form of the protein, as compared to the displacement observed experimentally and theoretically in murine Ngb, and concluded that this feature of Ngb might be protein-dependent. By probing an

alternative formation pathway for this same state, where the distal histidine–Fe bound is broken *before* the disulfide bridge is formed, we could obtain a new Pent-Cys_{ox}-bis state presenting structural characteristics much closer to the CO-bound murine Ngb, thus showing how the heme movement within the protein strongly depends on the thiols redox state. In particular, the formation of the disulfide bridge induces a notable reduction of the mobility of the CD and EF loops, and the heme sliding might be hindered in the more strained form of Ngb with oxidized thiols when trying to form a pentacoordinated state *after* building the internal disulfide bridge. This hypothesis is supported by 2D-IR spectroscopy experiments that showed how the intramolecular disulfide bond acts as an inhibitor of fast protein dynamics in human Ngb.⁷⁶ In addition, whereas the free-energy calculations of Nadra et al. showed how the existence of the internal disulfide bridge stabilizes the pentacoordinated

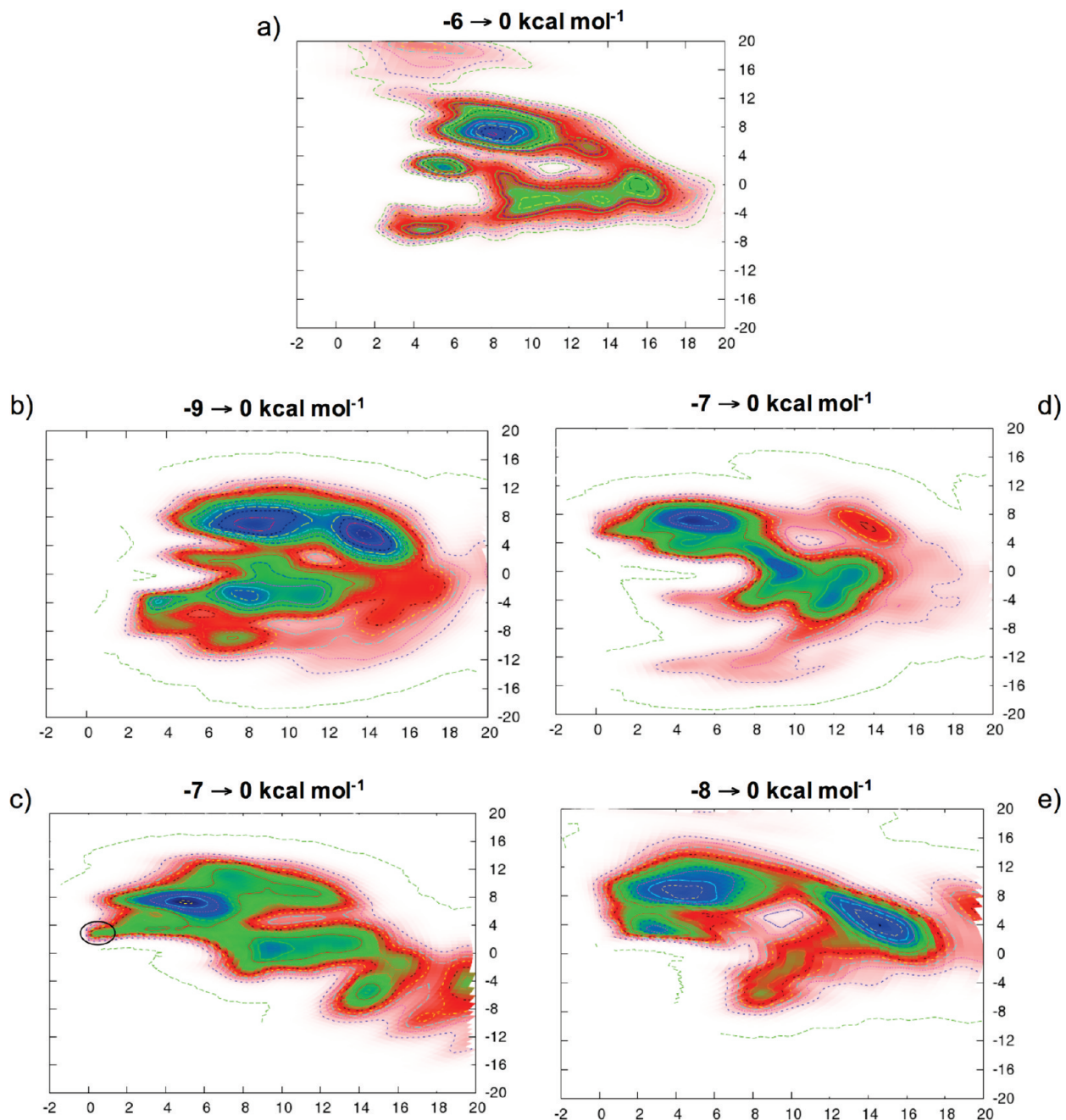


Figure 9. FESs of O_2 diffusion in Ngb. (a) Hex-Cys_{red} state, (b) Hex-Cys_{ox} state, (c) Pent-Cys_{ox} state, (d) Pent-Cys_{red} state, (e) Pent-Cys_{ox}-bis state. The black ellipse in part c highlights the ligand-bound configuration visited by O_2 during the simulation.

species, the FESs we obtained while constraining the S–S distance suggest that the internal disulfide bridge is, indeed, easier to form when the protein is in its pentacoordinated state. This result supports the idea of a complex interaction between these two characteristics of human Ngb.

The study of the internal cavity network of human Ngb shows the extreme plasticity of the interior of the protein, which displays extensive modifications when changing between species. These variations can notably be related to changes in the mechanical properties of the protein. For example, the Hex-Cys_{red}-to-Pent-Cys_{red} transition leads to a reorganization of the internal cavities toward the upper part of the protein with the appearance of an extended DP/Xe4 pocket (see Figure 2a and b). Meanwhile, the variation of the rigidity profile for this same transition shows an important decrease in the force constants of Phe28, Val68, and Val109, which are precisely located at

the frontier between the DP and Xe4 cavities, thus suggesting that the softening of these residues might facilitate the diffusion of a ligand from one pocket to the other.

In a second stage, we investigated the diffusion of three small gaseous ligands (CO , NO , and O_2) in the various states of human Ngb. The resulting FESs vary widely, depending on the ligand considered and protein state. However, the migration pathway can generally be related to the organization of the cavity network that has been observed earlier. The metadynamics trajectories also permitted location of eight passageways for the ligand toward the protein surface. Remarkably, all but one (exit 6) of these pathways had already been detected, either by structural studies of Ngb (exits 1 and 5), or by being related to ligand pathways obtained during simulations performed on Hb (exits 3 and 8) or Mb (exits 2, 3, 4, 7, and 8). These results support the idea of Cohen and Schulten⁴³ that, notwithstanding the

important variability of ligand migration pathways among members of the globin family, some specific residue positions within the globin fold could actually show a propensity to be located near a ligand passageway. The variation of the mechanical properties of the residues lining the exit passageways could also contribute to determination of the ligand escape trajectory. For example, the transition from the Hex-Cys_{red} to the Pent-Cys_{red} state of Ngb induces an important increase in the rigidity of Tyr137 (see Figure 2b, curve iii), thus blocking exit 1 in the pentacoordinated state for the CO ligand, which will instead use exit 3 to leave the protein.

Finally, we can note that for all three ligands, the occupation of the distal pocket with respect to the other cavities is favored in the pentacoordinated state with a disulfide bridge, which is in agreement with the calculations previously performed on human Ngb using the potential of mean force by the implicit ligand sampling method.⁴² However, whereas CO and NO will preferentially reside in the DP in the Pent-Cys_{ox}-bis state of Ngb, a ligand-bound configuration for O₂ in Ngb was observed only for the Pent-Cys_{ox} state. Overall, our results show that the ligand binding properties of this globin are controlled by a subtle interplay between the two specific features of human Ngb; namely, the hexa-to-penta-coordination transition and the formation of the disulfide bridge in the CD loop. In addition, the various migration pathways observed for the three ligands studied suggest that the formation mechanism of the pentacoordinated state with oxidized thiols (which seems to be the most favorable one for ligand binding) might be playing an important role in terms of ligand selectivity for the globin.

Acknowledgment. This work was granted access to the HPC resources of IDRIS under the allocation 2009-t2009086019 made by GENCI (Grand Equipement National de Calcul Intensif). The authors acknowledge Richard Lavery and Chantal Prévost for their thorough reading of the manuscript. A. Bocahut thanks Olivier Delalande for his help in setting up interactive simulations and fruitful discussions on molecular dynamics.

Supporting Information Available: The charges that were calculated for the heme group. This material is available free of charge via the Internet at <http://pubs.acs.org>.

References and Notes

- (1) Hardison, R. C. *Proc. Natl. Acad. Sci. U.S.A.* **1996**, *93*, 5675.
- (2) Vinogradov, S. N.; Hoogewijs, D.; Bailly, X.; Arredondo-Peter, R.; Gough, J.; Dewilde, S.; Moens, L.; Vanfleteren, J. R. *BMC Evol. Biol.* **2006**, *6*, 31.
- (3) Vinogradov, S. N.; Hoogewijs, D.; Bailly, X.; Mizuguchi, K.; Dewilde, S.; Moens, L.; Vanfleteren, J. R. *Gene* **2007**, *398*, 132.
- (4) Vinogradov, S. N.; Moens, L. *J. Biol. Chem.* **2008**, *283*, 8773.
- (5) Wajcman, H.; Kiger, L.; Marden, M. C. C. *R. Biol.* **2009**, *332*, 273.
- (6) Burmester, T.; Weich, B.; Reinhardt, S.; Hankein, T. *Nature* **2000**, *407*, 520.
- (7) Bashford, D.; Chothia, C.; Lesk, A. M. *J. Mol. Biol.* **1987**, *196*, 199.
- (8) Pesce, A.; Dewilde, S.; Nardini, M.; Moens, L.; Ascenzi, P.; Hankeln, T.; Burmester, T.; Bolognesi, M. *Structure* **2003**, *11*, 1087.
- (9) Vallone, B.; Nienhaus, K.; Brunori, M.; Nienhaus, G. U. *Proteins* **2004**, *56*, 85.
- (10) Dewilde, S.; Kiger, L.; Burmester, T.; Hankeln, T.; Baudin-Creuzza, V.; Aerts, T.; Marden, M. C.; Caubergs, R.; Moens, L. *J. Biol. Chem.* **2001**, *276*, 38949.
- (11) Pesce, A.; De Sanctis, D.; Nardini, M.; Dewilde, S.; Moens, L.; Hankeln, T.; Burmester, T.; Ascenzi, P.; Bolognesi, M. *IUMB Life* **2004**, *56*, 657.
- (12) Brunori, M.; Vallone, B. *FASEB J.* **2006**, *20*, 2192.
- (13) Brunori, M.; Vallone, B. *Cell. Mol. Life Sci.* **2007**, *64*, 1259.
- (14) Nienhaus, K.; Nienhaus, G. U. *IUMB Life* **2007**, *59*, 490.
- (15) Burmester, T.; Hankeln, T. *J. Exp. Biol.* **2009**, *212*, 1423.
- (16) Kriegl, J. M.; Bhattacharyya, A. J.; Nienhaus, K.; Deng, P. C.; Minkow, O.; Nienhaus, G. U. *Proc. Natl. Acad. Sci. U.S.A.* **2002**, *99*, 7992.
- (17) Brunori, M.; Giuffre, A.; Nienhaus, K.; Nienhaus, G. U.; Scandurra, F. M.; Vallone, B. *Proc. Natl. Acad. Sci. U.S.A.* **2005**, *102*, 8483.
- (18) Khan, A. A.; Mao, X. O.; Banwait, S.; Jin, K. L.; Greenberg, D. A. *Proc. Natl. Acad. Sci. U.S.A.* **2007**, *104*, 19114.
- (19) Watanabe, S.; Wakasugi, K. *Biochem. Biophys. Res. Commun.* **2008**, *369*, 695.
- (20) Giuffre, A.; Moschetti, T.; Vallone, B.; Brunori, M. *Biochem. Biophys. Res. Commun.* **2008**, *367*, 893.
- (21) Sun, Y. J.; Jin, K. L.; Mao, X. O.; Zhu, Y. H.; Greenberg, D. A. *Proc. Natl. Acad. Sci. U.S.A.* **2001**, *98*, 15306.
- (22) Greenberg, D. A.; Jin, K.; Khan, A. A. *Curr. Opin. Pharmacol.* **2008**, *8*, 20.
- (23) Sun, Y. J.; Jin, K. L.; Peel, A.; Mao, X. O.; Xie, L.; Greenberg, D. A. *Proc. Natl. Acad. Sci. U.S.A.* **2003**, *100*, 3497.
- (24) Vallone, B.; Nienhaus, K.; Matthes, A.; Brunori, M.; Nienhaus, G. U. *Proc. Natl. Acad. Sci. U.S.A.* **2004**, *101*, 17351.
- (25) Anselmi, M.; Brunori, M.; Vallone, B.; Di Nola, A. *Biophys. J.* **2007**, *93*, 434.
- (26) Anselmi, M.; Brunori, M.; Vallone, B.; Di Nola, A. *Biophys. J.* **2008**, *95*, 4157.
- (27) Hamdane, D.; Kiger, L.; Dewilde, S.; Green, B. N.; Pesce, A.; Uzan, J.; Burmester, T.; Hankeln, T.; Bolognesi, M.; Moens, L.; Marden, M. C. *J. Biol. Chem.* **2003**, *278*, 51713.
- (28) Nadra, A. D.; Marti, M. A.; Pesce, A.; Bolognesi, M.; Estrin, D. A. *Proteins* **2008**, *71*, 695.
- (29) Capece, L.; Marti, M. A.; Bidon-Chanal, A.; Nadra, A.; Luque, E. J.; Estrin, D. A. *Proteins: Struct., Funct., Bioinf.* **2009**, *75*, 885.
- (30) Tilton, R. F.; Kuntz, I. D.; Petsko, G. A. *Biochemistry* **1984**, *23*, 2849.
- (31) Brunori, M.; Gibson, Q. H. *EMBO Rep.* **2001**, *2*, 674.
- (32) Milani, M.; Pesce, A.; Ouellet, Y.; Ascenzi, P.; Guertin, M.; Bolognesi, M. *EMBO J.* **2001**, *20*, 3902.
- (33) Bourgeois, D.; Vallone, B.; Schotte, F.; Arcovito, A.; Miele, A. E.; Sciaro, G.; Wulff, M.; Anfinrud, P.; Brunori, M. *Proc. Natl. Acad. Sci. U.S.A.* **2003**, *100*, 8704.
- (34) Schotte, F.; Lim, M. H.; Jackson, T. A.; Smirnov, A. V.; Soman, J.; Olson, J. S.; Phillips, G. N.; Wulff, M.; Anfinrud, P. A. *Science* **2003**, *300*, 1944.
- (35) Bossa, C.; Anselmi, M.; Roccatano, D.; Amadei, A.; Vallone, B.; Brunori, M.; Di Nola, A. *Biophys. J.* **2004**, *86*, 3855.
- (36) Bossa, C.; Amadei, A.; Daidone, I.; Anselmi, M.; Vallone, B.; Brunori, M.; Di Nola, A. *Biophys. J.* **2005**, *89*, 465.
- (37) Mouawad, L.; Marechal, J. D.; Perahia, D. *Biochim. Biophys. Acta* **2005**, *1724*, 385.
- (38) Cohen, J.; Arkhipov, A.; Braun, R.; Schulten, K. *Biophys. J.* **2006**, *91*, 1844.
- (39) Ceccarelli, M.; Anedda, R.; Casu, M.; Ruggerone, P. *Proteins* **2008**, *71*, 1231.
- (40) Nishihara, Y.; Hayashi, S.; Kato, S. *Chem. Phys. Lett.* **2008**, *464*, 220.
- (41) Elber, R.; Gibson, Q. H. *J. Phys. Chem. B* **2008**, *112*, 6147.
- (42) Orlowski, S.; Nowak, W. *BioSyst.* **2008**, *94*, 263.
- (43) Cohen, J.; Schulten, K. *Biophys. J.* **2007**, *93*, 3591.
- (44) Berendsen, H. J. C.; Vanderspoel, D.; Vandrunen, R. *Comput. Phys. Commun.* **1995**, *91*, 43.
- (45) Lindahl, E.; Hess, B.; van der Spoel, D. *J. Mol. Model.* **2001**, *7*, 306.
- (46) Van der Spoel, D.; Lindahl, E.; Hess, B.; Groenhof, G.; Mark, A. E.; Berendsen, H. J. C. *J. Comput. Chem.* **2005**, *26*, 1701.
- (47) Kaminski, G. A.; Friesner, R. A.; Tirado-Rives, J.; Jorgensen, W. L. *J. Phys. Chem. B* **2001**, *105*, 6474.
- (48) Frisch, M. J.; Trucks, G. W.; Schlegel, H. B.; Scuseria, G. E.; Rob, M. A.; Cheeseman, J. R.; Montgomery, J. A., Jr.; Vreven, T.; Kudin, K. N.; Burant, J. C.; Millam, J. M.; Iyengar, S. S.; Tomasi, J.; Barone, V.; Mennucci, B.; Cossi, M.; Scalmani, G.; Rega, N.; Petersson, G. A.; Nakatsuji, H.; Hada, M.; Ehara, M.; Toyota, K.; Fukuda, R.; Hasegawa, J.; Ishida, M.; Nakajima, T.; Honda, Y.; Kitao, O.; Nakai, H.; Klene, M.; Li, X.; Knox, J. E.; Hratchian, H. P.; Cross, J. B.; Bakken, V.; Adamo, C.; Jaramillo, J.; Gomperts, R.; Stratmann, R. E.; Yazyev, O.; Austin, A. J.; Cammi, R.; Pomelli, C.; Ochterski, J. W.; Ayala, P. Y.; Morokuma, K.; Voth, G. A.; Salvador, P.; Dannenberg, J. J.; Zakrzewski, V. G.; Dapprich, S.; Daniels, A. D.; Strain, M. C.; Farkas, O.; Malick, D. K.; Rabuck, A. D.; Raghavachari, K.; Foresman, J. B.; Ortiz, J. V.; Cui, Q.; Baboul, A. G.; Clifford, S.; Ciosowski, J.; Stefanov, B. B.; Liu, G.; Liashenko, A.; Piskorz, P.; Komaromi, I.; Martin, R. L.; Fox, D. J.; Keith, T.; Al-Laham, M. A.; Peng, C. Y.; Nanayakkara, A.; Challacombe, M.; Gill, P. M. W.; Johnson, B.; Chen, W.; Wong, M. W.; Gonzalez, C.; Pople, J. A. *Gaussian 03*; Gaussian, Inc.: Wallingford, CT, 2003.
- (49) Lee, C. T.; Yang, W. T.; Parr, R. G. *Phys. Rev. B* **1988**, *37*, 785.
- (50) Li, H. Y.; Elber, R.; Straub, J. E. *J. Biol. Chem.* **1993**, *268*, 17908.
- (51) Miyamoto, S.; Kollman, P. A. *J. Comput. Chem.* **1992**, *13*, 952.

- (52) Berendsen, H. J. C.; Postma, J. P. M.; van Gunsteren, W. F.; DiNola, A.; Haak, J. R. *J. Chem. Phys.* **1984**, *81*, 3684.
- (53) Essmann, U.; Perera, L.; Berkowitz, M. L.; Darden, T.; Lee, H.; Pedersen, L. G. *J. Chem. Phys.* **1995**, *103*, 8577.
- (54) Hess, B.; Bekker, H.; Berendsen, H. J. C.; Fraaije, J. *J. Comput. Chem.* **1997**, *18*, 1463.
- (55) Garcia, A. E. *Phys. Rev. Lett.* **1992**, *68*, 2696.
- (56) Amadei, A.; Linssen, A. B. M.; Berendsen, H. J. C. *Proteins* **1993**, *17*, 412.
- (57) Case, D. A. *Curr. Opin. Struct. Biol.* **1994**, *4*, 285.
- (58) Amadei, A.; Linssen, A. B. M.; deGroot, B. L.; vanAalten, D. M. F.; Berendsen, H. J. C. *J. Biomol. Struct. Dyn.* **1996**, *13*, 615.
- (59) Hendlich, M.; Rippmann, F.; Barnickel, G. *J. Mol. Graphics Model.* **1997**, *15*, 359.
- (60) Sacquin-Mora, S.; Lavery, R. *Biophys. J.* **2006**, *90*, 2706.
- (61) Sacquin-Mora, S.; Laforet, E.; Lavery, R. *Proteins* **2007**, *67*, 350.
- (62) Zacharias, M. *Protein Sci.* **2003**, *12*, 1271.
- (63) Tozzini, V. *Curr. Opin. Struct. Biol.* **2005**, *15*, 144.
- (64) Ermak, D. L.; McCammon, J. A. *J. Chem. Phys.* **1978**, *69*, 1352.
- (65) Pastor, R. W.; Venable, R.; Karplus, M. *J. Chem. Phys.* **1988**, *89*, 1112.
- (66) Laio, A.; Parrinello, M. *Proc. Natl. Acad. Sci. U.S.A.* **2002**, *99*, 12562.
- (67) Laio, A.; Gervasio, F. L. *Rep. Prog. Phys.* **2008**, *71*, 126601.
- (68) Bonomi, M.; Branduardi, D.; Bussi, G.; Camilloni, C.; Provasi, D.; Raiteri, P.; Donadio, D.; Marinelli, F.; Pietrucci, F.; Broglia, R.-A.; Parrinello, M. *Comput. Phys. Commun.* **2009**, *180*, 1961.
- (69) Delalande, O.; Férey, N.; Grasseau, G.; Baaden, M. *J. Comput. Chem.* **2009**, *30*, 2375.
- (70) Barducci, A.; Bussi, G.; Parrinello, M. *Phys. Rev. Lett.* **2008**, *100*, 020603.
- (71) Raiteri, P.; Laio, A.; Gervasio, F. L.; Micheletti, C.; Parrinello, M. *J. Phys. Chem. B* **2006**, *110*, 3533.
- (72) Moschetti, T.; Mueller, U.; Schulze, J.; Brunori, M.; Vallone, B. *Biophys. J.* **2009**, *97*, 1700.
- (73) Savino, C.; Miele, A. E.; Draghi, F.; Johnson, K. A.; Sciaro, G.; Brunori, M.; Vallone, B. *Biopolymers* **2009**, *91*, 1097–1107.
- (74) Ptitsyn, O. B.; Ting, K. L. *J. Mol. Biol.* **1999**, *291*, 671.
- (75) Codutti, L.; Picotti, P.; Marin, O.; Dewilde, S.; Fogolari, F.; Corazza, A.; Viglino, P.; Moens, L.; Esposito, G.; Fontana, A. *FEBS J.* **2009**, *276*, 5177.
- (76) Ishikawa, H.; Kim, S.; Kwak, K.; Wakasugi, K.; Fayer, M. D. *Proc. Nat. Acad. Sci. U.S.A.* **2007**, *104*, 19309.
- (77) Humphrey, W.; Dalke, A.; Schulten, K. *J. Mol. Graph.* **1996**, *14*, 33.

JP906854X